Monthly Notices
of the
ROYAL ASTRONOMICAL SOCIETY

MNRAS **500,** 138–144 (2021)
Advance Access publication 2020 October 9

doi:10.1093/mnras/staa3057

Suppression of H_2-cooling in protogalaxies aided by trapped Lyα cooling radiation

Jemma Wolcott-Green[1]★ Zoltán Haiman[2] and Greg L. Bryan[2]
[1]Department of Physics, University of California Santa Barbara, MC 9530, Santa Barbara, CA 93106, USA
[2]Department of Astronomy, Columbia University, 550 West 120th Street, MC 5246, New York, NY 10027, USA

Accepted 2020 September 15. Received 2020 September 14; in original form 2020 January 20

ABSTRACT

We study the thermal evolution of UV-irradiated atomic cooling haloes using high-resolution three-dimensional hydrodynamic simulations. We consider the effect of H^- photodetachment by Lyα cooling radiation trapped in the optically-thick cores of three such haloes, a process that has not been included in previous simulations. Because H^- is a precursor of molecular hydrogen, its destruction can diminish the H_2 abundance and cooling. We find that the critical UV flux for suppressing H_2-cooling is decreased by ∼15–50 per cent in our fiducial models. Previous one-zone modelling found a larger effect, with $J_{\rm crit}$ reduced by a factor of a few; we show that adopting a constant halo mass to determine the trapped Lyα energy density, as is done in the one-zone models, yields a larger reduction in $J_{\rm crit}$, consistent with their findings. Our results nevertheless suggest that Lyα radiation may have an important effect on the thermal evolution of UV-irradiated haloes, and therefore on the potential for massive black hole formation.

Key words: molecular processes – stars: Population III – galaxies: formation – cosmology: theory – early Universe.

1 INTRODUCTION

It has long been known that H_2 is the primary coolant in primordial gas at temperatures below a few thousand Kelvin (Saslaw & Zipoy 1967). This has important implications for the first stars and protogalaxies, the reionization of the universe, and the formation of the first massive black holes (see Bromm & Yoshida 2011, for a review). Because H_2 is easily photodissociated by soft-UV photons in the Lyman–Werner (LW) bands (11.1–13.6 eV), radiation fields from the first stars can immediately have a strong feedback effect on their environments.

Photodissociation of H_2 has received particular attention in the context of gravitational collapse of haloes with virial temperatures $T_{\rm vir} \gtrsim 10^4$ K, in which gas is shock-heated to the virial temperature and can efficiently cool via atomic line cooling, even in the presence of a strong LW radiation field. These so-called atomic cooling haloes ('ACHs') have been proposed as possible hosts of the first supermassive black hole seeds. A variety of studies have shown that the presence of a strong LW photodissociating flux can prevent H_2-cooling during gravitational collapse in ACHs altogether, keeping the gas temperature near the virial temperature of the halo and thereby suppressing fragmentation on stellar-mass scales (see Inayoshi, Visbal & Haiman 2020, for a recent review). Subsequent rapid accretion rates on to a dense core ($\dot{M} \sim 0.1$–$1\ {\rm M}_\odot\ {\rm yr}^{-1}$), enabled by the elevated gas temperature, may lead to the formation of a massive (10^4–$10^6\ {\rm M}_\odot$) black hole seed via a supermassive star intermediary stage (Hosokawa, Omukai & Yorke 2012; Haemmerlé et al. 2018).

It is widely thought that in order for this so-called 'direct collapse' to occur, a large critical flux $J_{\rm crit}$ in the LW bands is required to suppress H_2-cooling (but see also Inayoshi, Li & Haiman 2018; Wise et al. 2019). Recent simulations have typically found $J_{\rm crit,\,21} = 10^3$–10^4, in the customary units $J_\nu = J_{21} \times 10^{-21} {\rm erg\ s^{-1}\ cm^{-2}\ Hz^{-1}\ sr^{1}}$ and normalized at the Lyman limit (Shang, Bryan & Haiman 2010; Latif et al. 2014, 2015; Regan, Johansson & Haehnelt 2014; Hartwig et al. 2015). In general, the critical flux depends sensitively on the shape of the irradiating spectrum (Agarwal et al. 2014; Sugimura, Omukai & Inoue 2014; Wolcott-Green, Haiman & Bryan 2017), H_2 self-shielding model (Wolcott-Green, Haiman & Bryan 2011; Hartwig et al. 2015), and rovibrational level populations (Wolcott-Green & Haiman 2019).

The effect of 'trapped' Lyman α (Lyα) photons on fragmentation has also been considered in this context. Neutral hydrogen column densities that build-up during gravitational collapse in ACHs exceed $N_{\rm H} \gtrsim 10^{21}\ {\rm cm}^{-2}$, and the resulting large optical depth in the Lyman series lines can suppress atomic cooling via Lyα in particular. Spaans & Silk (2006) suggested that this could lead to a stiffer equation of state than previously assumed, thus suppressing fragmentation. However, subsequent studies have shown that atomic cooling via other transitions, in particular H($2s \rightarrow 1s$), remains efficient even in dense cores where Lyα-cooling is strongly suppressed (e.g. Schleicher, Spaans & Glover 2010).

Recently, Johnson & Dijkstra (2017, hereafter JD17), used one-zone models to show that trapped Lyα photons may instead alter the thermal evolution of collapsing ACHs via photodetachment of H^-, an intermediary in the primary formation reaction for H_2:

$$H^- + H \rightarrow H_2 + e. \tag{1}$$

H^- can be destroyed by photons with $E > 0.76$ eV, but previous studies have considered photodetachment only by the incident radiation field. JD17 found that while *Lyα photons alone do not suppress H_2 abundance enough to prevent molecular cooling*, when this additional photodetachment is included with an incident photodissociating flux, *the critical LW flux is decreased by up to a factor*

★ E-mail: jemma@physics.ucsb.edu

Published by Oxford University Press on behalf of the Royal Astronomical Society

of ≈*5*. Such a reduction in $J_{\rm crit}$ would have important implications for the number density of direct collapse candidates, since the number of haloes exposed to a supercritical flux increases exponentially with decreasing $J_{\rm crit}$ (Dijkstra et al. 2008).

The goal of this study is to implement H$^-$-photodetachment by trapped Lyα in a suite of three-dimensional hydrodynamic simulations in order to further understand and quantify the magnitude of any reduction of $J_{\rm crit}$ in atomic cooling haloes. We use the publicly-available ENZO code to simulate three such haloes with and without the additional H$^-$-photodetachment by trapped Lyα, and further compare the results using different estimates for the trapped Lyα energy density produced during gravitational collapse.

In one set of simulations, we adopt the same approximation for the Lyα energy density as in JD17 and find a similar reduction in the critical flux as found in their one-zone models: $J_{\rm crit}({\rm Ly}\alpha)/J_{\rm crit,\,0} \sim$ 0.2–0.8. We also show, however, by post-processing the simulations that their model may overestimate the amount of Lyα produced in our haloes once the gas density reaches $n \approx$ 10–100 cm^{-3}, a key stage in the collapse determining whether H$_2$-cooling is suppressed. Adopting a more conservative model for the trapped Lyα intensity results in a more modest reduction in the critical flux, $J_{\rm crit}({\rm Ly}\alpha)/J_{\rm crit,\,0}$ = 0.5–1. Our results nevertheless suggest that trapped Lyα may be important in the thermal evolution of UV-irradiated ACHs. A more detailed treatment of Lyα radiative transfer is needed to precisely determine the photodetachment rate and the resulting decrease in the critical flux.

This paper is organized as follows: We describe the numerical modeling in Section 2 and discuss the results in Section 3. We summarize our primary findings and offer conclusions in Section 4.

2 NUMERICAL MODELLING

2.1 Numerical modeling

We use ENZO,[1] a publicly-available adaptive mesh refinement code, which uses an N-body adaptive particle mesh technique to follow the dark matter (DM) dynamics, and a second-order accurate piecewise parabolic method to solve the hydrodynamics (see Bryan et al. 2014, for an in-depth description of the modelling). We use the nine-species non-equilibrium chemistry network in ENZO to follow the chemical evolution of gas with primordial composition. Radiative cooling by H$_2$ is modelled with the cooling function from Galli & Palla (1998). We also updated several of the reaction rates in the default ENZO chemistry network, as detailed in Appendix A.

Initial conditions for a simulation volume 1h^{-1} Mpc on a side and 128^3 root grid are generated with the MUSIC[2] package (Hahn & Abel 2011). We initialize the simulation at $z_{\rm in} = 99$ and adopt the cosmological parameters from the Planck 2018 collaboration (Planck Collaboration VI 2018), $\Omega_{\rm m} = 0.315$, $\Omega_\Lambda = 0.685$ $\Omega_{\rm b} = 0.0493$, $h = 0.674$, $\sigma_8 = 0.811$, and $n = 0.965$.

In order to select haloes for ‘zoom-in’ simulations, we run an initial low-resolution DM-only simulation from $z_{\rm in} = 99$ to 10, with a maximum of four levels of refinement. The ROCKSTAR halo finder (Behroozi, Wechsler & Wu 2013) is run to find haloes with $T_{\rm vir} \gtrsim 10^4$ K at $z = 10$. Initial conditions are then re-generated with three nested grids enclosing the Lagrangian volume of the selected halo. With the additional nested grids, the most refined region has an effective grid resolution of 1024^3 and DM particle mass ∼100 M$_\odot$.

Table 1. Mass and virial temperature of haloes A–C at the collapse redshift with $J = J_{\rm crit}$ (no H$^-$ photodetachment by Lyα.).

	Halo A	Halo B	Halo C
$z_{\rm coll}(J_{\rm crit})$	11.87	13.26	9.36
$M_{\rm tot}/10^7$ M$_\odot$ ($z_{\rm coll}$)	1.9	1.4	2.1
$T_{\rm vir}/10^3$ K ($z_{\rm coll}$)	7.9	7.2	6.7

High-resolution zoom simulations for three of the selected haloes are run from $z_{\rm in} = 99$ with the maximum refinement level set to 18, resulting in a minimum cell size of 0.0298 h^{-1} cpc. The redshift when the simulation reaches this maximum refinement is referred to as the collapse redshift, $z_{\rm coll}$. In order to avoid numerical effects of discrete DM particles, the DM distribution is smoothed at a maximum refinement level of 13. Cells are flagged for additional spatial refinement when the baryon or DM mass is four times greater than that of the most refined cell. In addition, the local Jeans length is always resolved by at least 16 cells in order to avoid spurious fragmentation (Truelove et al. 1997). The properties of all three haloes at their collapse redshift with $J_{21} > J_{\rm crit}$ are shown in Table 1.

2.2 Implementing H$^-$ photodetachment by Lyα

In our first set of simulations including H$^-$ photodetachment by trapped Lyα, we utilize the model described by Johnson & Dijkstra (2017, see their equations 3–7), and briefly summarized here. They assume the energy radiated in Lyα cooling radiation balances the gravitational binding energy released by a cloud of mass $M = 10^6$ M$_\odot$ collapsing on a free-fall time-scale.

The derived Lyα energy density u_α accounts for the increased path-length of a photon escaping an optically-thick medium,

$$u_\alpha = M_F \times \frac{L_{\rm Ly\alpha} r_{\rm cloud}}{V_{\rm cloud} c}, \qquad (2)$$

where $L_{\rm Ly\alpha}$ is the luminosity from the simple toy model above, $r_{\rm cloud}$ is the size of the cloud, $V_{\rm cloud}$ is the geometrical volume of the cloud, c is the speed of light, and $M_F \sim (a_v \tau_{\rm Ly\alpha})^{1/3}$ is the dimensionless path-length boost. For this boost, a_v denotes the Voigt profile, $\tau_{\rm Ly\alpha} = 5.9 \times 10^6 (N_{\rm H}/10^{20}~{\rm cm}^{-2})(T/10^4{\rm K})^{1/2}$ is the line-center optical depth, and $N_{\rm H}$ is the neutral hydrogen column density, found by assuming a cloud of uniform density. For an isotropic Lyα field within the cloud and using the cross-section for photodetachment, $\sigma_{\rm H^-} = 5.9 \times 10^{-18}$ cm^2 at $E_{\rm Ly\alpha} = 10.2$ eV, they derive the photodetachment rate:

$$R_{\rm det} \simeq 10^{-8}{\rm s}^{-1} \left(\frac{M}{10^6~{\rm M}_\odot}\right)^{10/9} \left(\frac{T}{10^4~{\rm K}}\right)^{-1/3} \times \left(\frac{n}{10^2~{\rm cm}^{-3}}\right)^{31/18} \left(\frac{B_\alpha}{2}\right), \qquad (3)$$

where n is the density. The parameter B_α is included by JD17 in their one-zone models to capture the possible impact of density gradients and non-uniform spatial diffusion of Lyα photons (see their Appendix A). This does not translate directly in the case of our three-dimensional simulations; however, we retain the same B_α notation and simply treat it as a free parameter, accounting for uncertainty in the Lyα energy density in this simple model (see Section 3.2 for more details on the value of B_α). The set of simulations we run with this rate (directly from JD17) will be referred to as ‘constant mass’ models.

In order to evaluate the validity of this one-zone model prescription for our simulated haloes, we have examined the enclosed mass profiles at several redshift snapshots in our haloes up to the collapse

---

[1] http://enzo-project.org.

[2] www-n.oca.eu/ohahn/MUSIC/.

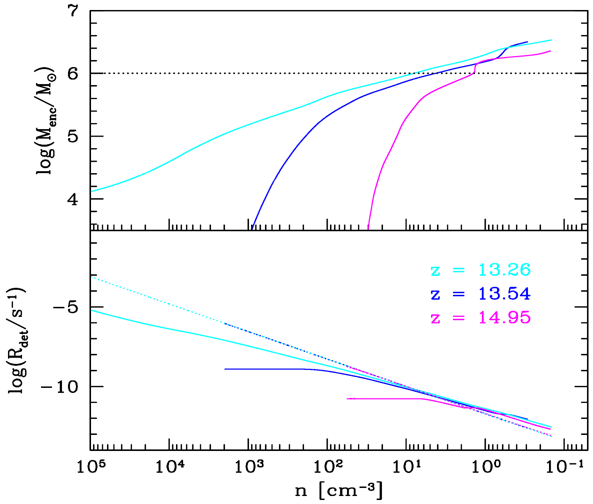

Figure 1. Top panel: enclosed mass profile $M_{\rm enc}(< r, z)$ for Halo B as a function of spherically-averaged density $n(r)$, shown at $z_{\rm coll}$ (when the simulation reaches its maximum density), and two additional redshifts prior to collapse. Bottom panel: H^- photodetachment rate due to trapped Lyα cooling radiation (see equation 3) assuming a fixed mass, $M = 10^6$ $M_\odot$ (dotted), or enclosed mass, $M_{\rm enc}(< r, z_{\rm coll})$ (solid).

redshift. These are shown for one of the haloes in the top panel of Fig. 1. Because the density profiles toward the core are relatively steep, the enclosed mass $M(< r, z)$ at $n \gtrsim 10^2$ cm^{-3} falls rapidly below 10^6 $M_\odot$. As a result, the photodetachment rate with fixed $M = 10^6$ $M_\odot$, as in JD17, is significantly larger than if the actual enclosed mass $M(< r, z)$ is instead used in equation (3), as shown in the lower panel of Fig. 1.

Using $R_{\rm det}$ with $M(< r, z)$ self-consistently in the simulation would unfortunately require that we compute the density profile on the fly, which is beyond the scope of the current modeling. Instead, we run a set of simulations assuming $M = M(< r, z_{\rm coll})$, which we will refer to as the 'enclosed mass' models. While this is still larger than $M(< r, z)$ at earlier redshifts, it is sufficient for the purposes of the relatively simple model used to estimate the Lyα radiation field.

It is worth noting that this model assumes a static cloud; in reality, bulk motions within the collapsing gas scatter Lyα photons away from line center, potentially reducing the effective column density and the trapped Lyα energy density. However, in the haloes we study, the minimum line-of-sight column densities within the collapsing cores are $\gtrsim 10^{19}$–10^{20}cm^{-2} once the critical density is reached, $n \sim 10^3$–10^4 cm^{-3}, above which many of the rovibrational states of H_2 reach LTE and the total dissociation rate becomes dominated by collisional dissociation (see, e.g. section 3.4 in Shang et al. 2010, for a detailed discussion). For a gas at $\sim 10^4$ K, this means that the gas is optically thick well into the line wings (see, e.g. fig. 17 in Dijkstra 2019, which shows that the line remains optically thick even 200–400 km s^{-1} away from the line center). We do not expect the effective optical depth to be significantly reduced by bulk motions of the gas at the inflow speeds that are of order 10 km s^{-1}.

2.3 Incident radiation field

2.3.1 Photodissociation of molecular hydrogen

We adopt the commonly used approach for modeling an incident H_2-photodissociating flux with a blackbody spectrum with $T_* = 10^5$ K up to the Lyman limit. Ionizing photons are assumed to have been absorbed,[3] likely by neutral gas within the irradiating galaxy itself. While the Pop III IMF remains uncertain, the H_2 photodissociation rate derived with this spectrum is a good approximation for metal-free starburst populations (e.g. Wolcott-Green et al. 2017). We use the fitting formula for the optically-thick H_2 photodissociation rate from Wolcott-Green et al. (2011) in order to directly compare to the JD17 results; note that this fit was recently updated by Wolcott-Green & Haiman (2019) to significantly improve the accuracy for vibrationally warm H_2 ($T \gtrsim 3000$ K, $n \gtrsim 10^3$ cm^{-3}). Using the updated fit would likely yield a modest decrease in self-shielding (and therefore in $J_{\rm crit}$). The self-shielding H_2 column density is estimated with a local 'Sobolev-like' length as the characteristic length scale:

$$L_{\rm char} = \frac{\rho}{\nabla \rho}, \tag{4}$$

$$N_{H_2} = n_{H_2} \times L_{\rm char}. \tag{5}$$

This has been previously implemented in the ENZO network, and Wolcott–Green et al. (2011) showed it is a more accurate local prescription than the oft-used Jeans length.

Table 2. Critical fluxes in units $J_{\rm crit,\,21}/10^3$ for haloes A–C, with and without H^- photodetachment by trapped Lyα.

		Constant mass		Enclosed mass	
B_α	0	1	10	1	10
Halo A	6	3	2	5	3
Halo B	12	4	2	11	10
Halo C	7	6	2	7	4

Notes. Results are shown for constant mass, $M = 10^6 M_\odot$, and enclosed mass, $M(< r, z_{\rm coll})$, models. The top row shows the value of the factor B_α, which scales the trapped Lyα photon density to allow for non-uniform density profiles and photon-diffusion (see equation 3).

2.3.2 Photodetachment of H^- *by incident radiation field*

While H^- photodetachment by the incident flux is not the dominant mechanism for H_2-suppression with a 10^5-K blackbody spectrum, it is included in our modelling with the standard rate coefficient: $k_{H^-} = 1.07 \times 10^{-11} J_{21}$ cm^3 s^{-1}.

3 RESULTS AND DISCUSSION

3.1 Impact of H^- detachment by trapped Lyα

In order to determine the critical flux for each of the haloes and Lyα models, we run the zoom simulations for each with a series of incident flux strengths. The initial runs with $J_{21} = 10^3$, 5×10^3, 10^4 were analyzed at the collapse redshift to determine if H_2-cooling was suppressed. Subsequently, a set of more finely spaced flux tests (increments of 10^3 in J_{21}) were run to precisely determine $J_{\rm crit}$ required to prevent cooling below $T \approx T_{\rm vir}$.

The resulting critical fluxes for each of our haloes and Lyα models are listed in Table 2. In the $B_\alpha = 0$ cases, the only H^--photodetachment is from the incident radiation. For these, $J_{\rm crit,\,21}$

---

[3] We do not include the characteristic saw-tooth modulation seen in the cosmological LW background spectrum as a result of absorption in the IGM (Haiman, Abel & Rees 2000). The critical LW flux, $J_{\rm crit}$, is much larger than the expected cosmological background, and is most likely to originate instead from a bright near neighbour galaxy (Visbal, Haiman & Bryan 2014; Regan et al. 2017).

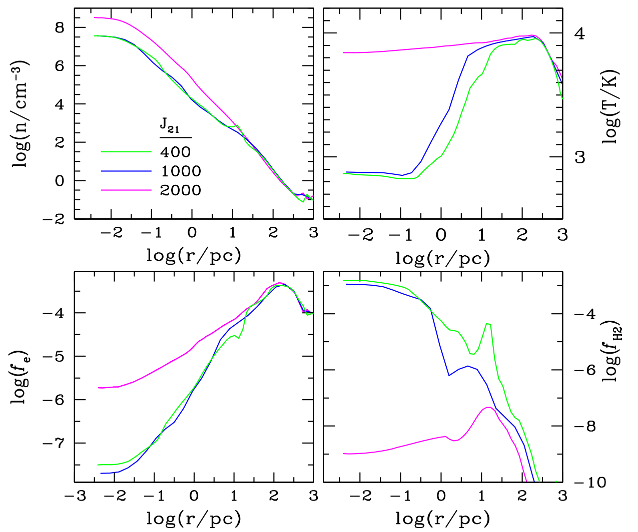

Figure 2. The profiles of spherically-averaged density (upper left-hand panel), temperature (upper right-hand panel), electron, and H$_2$ fractions (lower left- and right-hand panels, respectively) for Halo A. All profiles are at the collapse redshift of each simulation, and for varied intensity of the incident LW radiation: $J_{21} = 400$, 1000, 2000.

in the three haloes is found to be in the range (6–12)× 10^3. This is a factor of ∼5–10 larger than the one-zone results in JD17. Previous studies have also found a larger critical flux in simulations; this is attributed to hydrodynamic effects including shocks, which can increase the ionization fraction, and are not captured by the one-zone modeling (e.g. Shang et al. 2010; Latif et al. 2014, 2015). The halo-to-halo $J_{\rm crit}$ variation is also consistent with previous studies, which is often found to be within a factor of approximately 3.

We show in Fig. 2 the spherically-averaged density and temperature profiles[4] at the collapse redshift for one of our simulated haloes, as well as the fractional abundances of electrons and H$_2$. Each panel shows the results (in halo A) for varied $J_{21} = (0.2, 0.5, 1.0)J_{\rm crit}(B_\alpha = 10)$. The results follow the typical pattern seen in previous simulations of LW-irradiated ACHs: With subcritical flux, the H$_2$-fraction in the dense core reaches the standard ‘freeze-out’ value $\sim 10^{-3}$ (Oh & Haiman 2002), resulting in robust H$_2$-cooling and gas temperatures of a few hundred Kelvin in the inner $r \sim 0.1$pc. Once the critical flux is reached, the H$_2$-fraction is suppressed, $f_{\rm H_2} \lesssim 10^{-7}$, and the gas temperature remains near the virial temperature of the halo ≈7000 K.

3.2 Enclosed mass models

In our fiducial models using the ‘enclosed mass’ M($< r$, $z_{\rm coll}$) to estimate the Lyα energy density, we find that the inclusion of Lyα-photodetachment decreases $J_{\rm crit}$ in two of the three haloes (A and B) very modestly – by ∼10–15 per cent with $B_\alpha = 1$. In the $B_\alpha = 10$ case, all three haloes see a decrease in $J_{\rm crit}$, ranging from ∼15 to 50 per cent (see Table 2).

Even with the modified rate using the enclosed mass, this is a somewhat crude model for estimating the Lyα energy density. For the sake of a ‘sanity check’, in Fig. 3, we show the photodetachment rate with Lyα energy density obtained directly from the volume-integrated atomic cooling rate (rather than based on the gravitational binding energy released in a free-fall time, as previously). As shown in the top panel, this ‘$R_{\rm cool}$’ rate (solid lines) mostly lies between our enclosed-mass models with $B_\alpha = 1$ and 10 (dotted and dashed lines, respectively). The exception is at the final snapshot, $z_{\rm coll}$, when $R_{\rm cool}$ is significantly larger than even the $B_\alpha = 10$ model at densities below ~ 100 cm^{-3}.

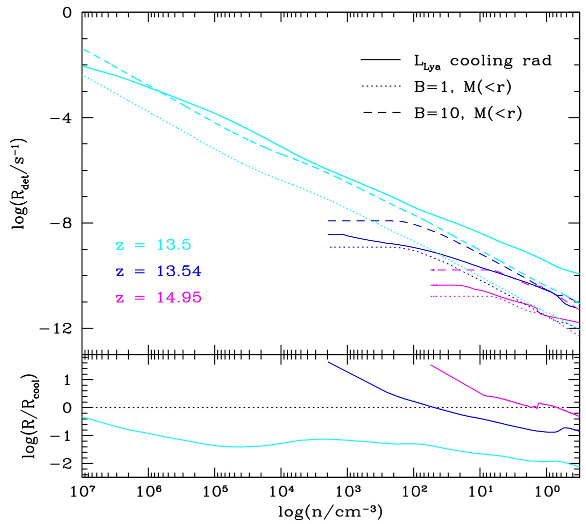

Figure 3. Top panel: the photodetachment rate of H$^-$ for Halo B at several redshifts, using equation (3) with the enclosed mass and $B_\alpha = 1$ and 10 (dotted and dashed lines, respectively). The solid line shows the same using the volume integrated cooling rate to derive a Lyα luminosity (rather than based on gravitational binding energy release in a free-fall time, as in JD17). Bottom panel: ratio of the photodetachment rate using the $B_\alpha = 1$ M ($< r$, $z_{\rm coll}$) model (dotted cyan line in the upper panel) to that from the Lyα cooling radiation calculated at each redshift (solid lines in the upper panel). This comparison is shown because the former is used in one set of simulations (see Table 2).

This rough agreement with the $B_\alpha = 1$, 10 rates is reassuring that the model employed here yields a reasonable estimate for $R_{\rm det}$; however, as discussed in Section 2.2, the rate implemented in our simulations actually is obtained using $M(< r, z_{\rm coll})$, since we do not track the enclosed mass on the fly (see Section 2). Therefore, the rates implemented in our ENZO network are the $z = 13.5$ curves (cyan) with $B_\alpha = 1$ and 10 (dotted and dashed).

The ratio of the $B_\alpha = 1$ rate with $R_{\rm cool}$ is shown in the lower panel of Fig. 3. At the pre-collapse redshifts, where $n_{\rm max} \approx 10^2$–10^3 cm^{-3}, our implemented rate with $M(< r, z_{\rm coll})$ diverges from $R_{\rm cool}$ at $n \sim 10$–100 cm^{-3} and becomes ∼ an order of magnitude larger at the highest densities. By the time the collapse has reached $n_{\rm max} = 10^7$ cm^{-3} at $z_{\rm coll}$, $R_{\rm cool}$ is much smaller than the original rate with $B_\alpha = 1$. This, suggests that our models may underestimate the trapped Lyα intensity, especially at very high densities. A more detailed study of the radiative transfer is needed in order to more precisely determine the photodetachment rates in a collapsing halo.

We note that there is a strong dependence of the predicted number of candidate haloes on $J_{\rm crit}$. For example, using the PDF in Ahn et al. (2009) for a rough estimate, a 10–50 per cent reduction in $J_{\rm crit}$ can increase the number of candidate haloes by a factor of approximately 2–5. We note, however, that the flux PDF sampled by haloes is uncertain. Chon et al. (2016), which includes subhaloes and smaller minihaloes, finds a much flatter PDF (see their fig. 1). It is unclear if most of these low-mass haloes can collapse and

---

[4] We use the publicly-available package YT (Turk et al. 2011) for simulation data analysis and visualization; see yt-project.org.

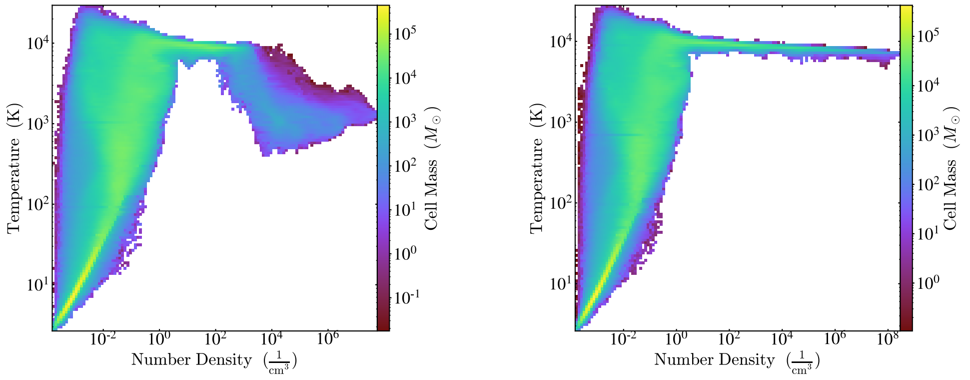

Figure 4. Phase diagrams of the subcritical (left-hand panel) and supercritical (right-hand panel) runs in Halo A shown at the collapse redshift ($B_\alpha = 1$).

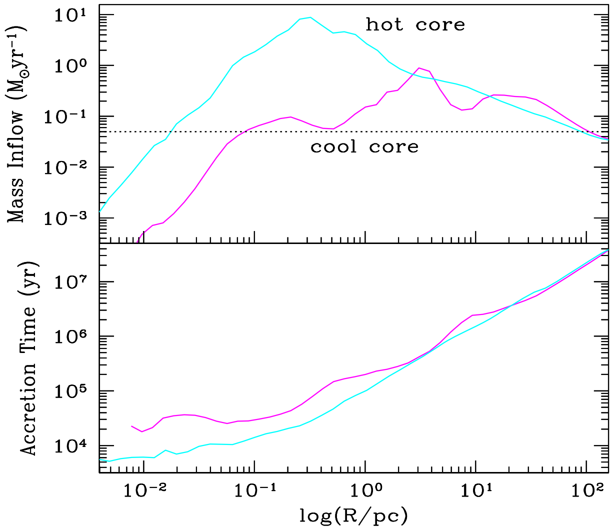

Figure 5. Lower panel: the local accretion time-scale $\equiv R/\langle v_{\rm rad}\rangle$is shown for Halo A at the collapse redshift ($z = 11.9$) in the case of a supercritical flux, which prevents H_2-cooling (cyan curve), and subcritical flux (magenta curve) in which the gas is able to cool via H_2. Upper panel: rate of mass inflow ($\dot{M} = 4\pi R^2 \rho \langle v_{\rm rad}\rangle$) is shown for the same halo snapshot as the lower panel. The 'critical' inflow rate is marked with a dotted horizontal line. At the relevant radii for direct collapse, ~0.1–0.3 pc (see Section 3.4), the inflow safely exceeds this threshold rate only in the case of the supercritical flux (hot core). The results are qualitatively similar for the other haloes and therefore have been omitted here for clarity.

produce LW radiation in the face of tidal forces and ram pressure stripping (see, e.g. fig. 8 and related discussion in Inayoshi et al. 2020). If we nevertheless use this flatter PDF for a rough estimate, reducing $J_{\rm crit}$ by ~40 per cent – as in Halo C – leads to an ~75 per cent increase in the predicted number of candidate haloes for direct collapse.

3.3 Constant mass models

In the 'constant mass' models, the photodetachment rate by trapped Lyα is identical to that implemented by JD17 (equation 3 above, $M = 10^6$ M$_\odot$); for direct comparison to JD17, we run two sets of models with $B_\alpha = 1$ and 10. The critical flux in the $B_\alpha = 1$ case is decreased by a factor of 2–3 in Haloes A and B, while in Halo C, it is reduced by only ~15 per cent compared to $B_\alpha = 0$. The latter is similar to the ~18 per cent reduction found by JD17 in their one–zone models.

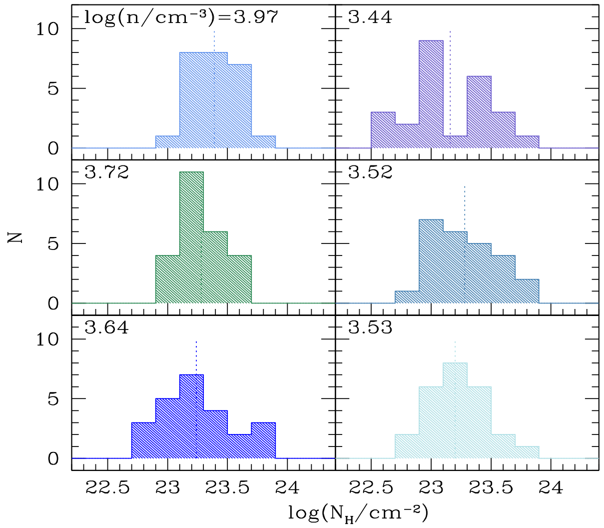

Figure 6. Each panel shows the neutral hydrogen column density along 25 different sightlines emanating from a location in Halo A, located ~5 pc from the densest part of the core. The mean $N_{\rm H\,I}$ for each point is shown by a vertical dotted line. Local particle densities at each point are indicated on the figure.

In our models with $B_\alpha = 10$, the critical flux is decreased further: $J_{\rm crit}(B_\alpha = 10)/J_{\rm crit,\,0} = 0.33$, 0.17, and 0.29 in Haloes A, B, and C, respectively. This is as expected, since the Lyα detachment rate is larger, and is also consistent with the JD17 results, in which $J_{\rm crit}(B_\alpha = 10) \approx 0.18 J_{\rm crit,\,0}$.

The decrease in $J_{\rm crit}$ is larger here than in the enclosed mass models. This is as expected, since the enclosed mass in the region where $n \gtrsim 10$ cm^{-3} is less than 10^6 M$_\odot$ (see Fig 1 and Table 1); therefore, the enclosed mass model yields a smaller Lyα energy density than the constant mass case at the stages of collapse that are key for determining the critical flux.

Example phase diagrams of number density and temperature at $z_{\rm coll}$ (for Halo A and $B_\alpha = 1$) are shown in Fig 4; in the left-hand panel, the flux was subcritical ($J_{21} = 2/3 J_{\rm crit}$) and the right-hand panel shows results with a supercritical flux. These too are consistent with the results of previous studies; in particular, the subcritical case shows that the shock-heated gas remains at $\sim T_{\rm vir}$ during the collapse until the density reaches 10^2–10^3 cm^{-3}, at which point the H_2 formation time becomes smaller than the dissociation time-scale, and the gas then cools (see, e.g. Shang et al. 2010, for an in-depth discussion of the relevant time-scales determining $J_{\rm crit}$).

3.4 Gas inflow rate and mass of the final object

The rate of gas inflow on to the core in ACHs is a key factor in determining the mass of the central object that can form (e.g. Inayoshi et al. 2020, and citations therein). A 'critical' mass inflow rate required for SMS formation has been found to be $\sim 0.05\,\mathrm{M}_{\odot}\,\mathrm{yr}^{-1}$ (Hosokawa et al. 2013; Schleicher et al. 2013; Haemmerlé et al. 2018).

In Fig. 5, we show the mass inflow rate (upper panel) ($\dot{M} = 4\pi R^2 \rho \langle v_{\rm rad} \rangle$) for Halo A at the collapse redshift in the case of a supercritical (cyan) and subcritical (magenta) flux. As expected, in the supercritical case (with $T_{\rm gas} \sim T_{\rm vir}$) the mass inflow rate is significantly higher (by up to two orders of magnitude) than in the subcritical case, in which the gas has cooled via H_2.

In the lower panel of Fig. 5, the local accretion time-scale ($t_{\rm acc} \equiv R/\langle v_{\rm rad} \rangle$) is shown for the same halo snapshot. For metal-free gas contracting on a Kelvin–Helmholtz time-scale of $\sim 10^4$–10^5 yr, the relevant radii, where $t_{\rm acc} \gtrsim t_{\rm KH}$, are ~0.1–0.3 pc. At these radii, the mass inflow rate safely exceeds the critical rate only in the case of the supercritical flux. These results are consistent with previous studies, which typically find that haloes in which H_2-cooling is suppressed are more likely to maintain high accretion rates and accumulate up to 10^4–$10^5\,\mathrm{M}_{\odot}$ of gas within the Kelvin–Helmholtz time.

3.5 Neglected processes

3.5.1 *Depletion of Lyα by vibrationally warm* H_2

There are several H_2 Lyman transitions that lie close to the Lyα line center; therefore, in a gas with a significant H_2 fraction, Lyα can be systematically converted into H_2 fluorescent emission. Neufeld (1990) showed that a large fraction of Lyα photons are thus converted when the $v = 2$, $J = 5, 6$ states are thermally populated and the gas temperature is $\gtrsim$ a few thousand Kelvin. For example, in a cloud with $N_{\rm H} = 10^{20}\,\mathrm{cm}^{-2}$ and H_2 fraction $f_{\rm H2} = 10^{-3}$, >90 per cent of Lyα (emitted by a central source) are converted into H_2 Lyman band radiation (via the B-X 1-2P[5] and B-X 1-2R[6] transitions), before they can escape the cloud.

JD17 assume that this process is unimportant since the H_2 fraction in gas exposed to a near-critical flux is small, $f_{\rm H2} \sim 10^{-7}$. Further, they point out that even if Lyα photons are absorbed by vibrationally-warm H_2, most of these events will result in a fluorescent radiative cascade, releasing additional photons that can photodetach H^-. We note that it is also possible that this Lyα pumping of H_2 could directly contribute to the photodissociation rate and thus further suppress the H_2 abundance; however, a detailed accounting of this process is beyond the scope of this work.

3.5.2 *Anisotropic H I column densities*

All of the results we present are based a model that assumes isotropic H I column densities. In more detailed radiative transfer modeling, there will be lower column-density sightlines via which Lyα photons can escape more easily, potentially reducing the trapping time and thus the energy density of Lyα in the core. While a detailed treatment of this is beyond the scope of our present work, it is worth considering the magnitude of the possible effect on our results. We show in Fig. 6 the column densities along 25 sightlines, emanating from six different points in one of our haloes. All six points are chosen to be located ~5 pc from the densest point in the core (at $z_{\rm coll}$). The mean $N_{\rm H\,I}$ is shown by a vertical dotted line in each panel, and in each case, the mean is only a factor of ~ a few larger than the lowest column density sightline. Because $R_{\rm det} \propto N_{\rm H\,I}^{1/3}$, we expect the change due to low column density sightlines would be relatively small. The difference in our results for $B_{\alpha} = 1$ and 10 is significantly larger than the variations that we would expect be introduced by anisotropic column densities.

4 CONCLUSIONS

We have run a suite of high-resolution 3D hydrodynamic simulations to study the effect of trapped Lyα cooling radiation on the thermal evolution of UV-irradiated atomic cooling haloes. We show that the critical UV flux for suppressing H_2-cooling is decreased by up to a factor of ≈5 when H^- photodetachment by Lyα is included with a simple high-end estimate of the trapped Lyα photon density. In models with a more conservative estimate of the trapped Lyα energy density, we find the critical flux is decreased by ~15–50 per cent. Our results are consistent with previous one-zone models (Johnson & Dijkstra 2017) and suggest that Ly α radiation may have an important effect on the thermal evolution of UV-irradiated haloes. While we have implemented two different models for the trapped Lyα energy density, there remains significant uncertainty due to the difficulty of accurately computing this quantity on the fly in simulations. This should be addressed in future work through a more detailed treatment of Lyα radiative transfer.

ACKNOWLEDGEMENTS

This material is based upon work supported by the National Science Foundation under Award No. 1903935. JWG is grateful to Cameron Hummels for useful discussions about the simulation set-up. ZH and GB acknowledge support from NSF grant NNX15AB19G. GLB acknowledges support from NSF grants AST-1615955 and OAC-1835509. We thank the anonymous referee for comments that helped to improve this paper.

DATA AVAILABILITY

The data underlying this paper will be shared on reasonable request to the corresponding author.

REFERENCES

Abel T., Anninos P., Zhang Y., Norman M. L., 1997, Nature, 2, 181
Agarwal B., Dalla Vecchia C., Johnson J. L., Khochfar S., Paardekooper J.-P., 2014, MNRAS, 443, 648
Ahn K., Shapiro P. R., Iliev I. T., Mellema G., Pen U., 2009, ApJ, 695, 1430
Behroozi P. S., Wechsler R. H., Wu H.-Y., 2013, ApJ, 762, 109
Bromm V., Yoshida N., 2011, ARA&A, 49, 373
Bryan G. L. et al., 2014, ApJS, 211, 19
Chon S., Hirano S., Hosokawa T., Yoshida N., 2016, ApJ, 832, 134
Dijkstra M., 2019, Lyman-alpha as an Astrophysical and Cosmological Tool, Saas-Fee Advanced Course. Springer-Verlag, Berlin
Dijkstra M., Haiman Z., Mesinger A., Wyithe J. S. B., 2008, MNRAS, 391, 1961
Galli D., Palla F., 1998, A&A, 335, 403
Glover S. C. O., 2015a, MNRAS, 451, 2082
Glover S. C. O., 2015b, MNRAS, 453, 2901
Haemmerlé L., Woods T. E., Klessen R. S., Heger A., Whalen D. J., 2018, MNRAS, 474, 2757
Hahn O., Abel T., 2011, MNRAS, 415, 2101
Haiman Z., Abel T., Rees M. J., 2000, ApJ, 534, 11
Hartwig T., Glover S. C. O., Klessen R. S., Latif M. A., Volonteri M., 2015, MNRAS, 452, 1233

Hosokawa T., Omukai K., Yorke H. W., 2012, ApJ, 756, 93
Hosokawa T., Yorke H. W., Inayoshi K., Omukai K., Yoshida N., 2013, ApJ, 778, 178
Hutchins J. B., 1976, ApJ, 205, 103
Inayoshi K., Li M., Haiman Z., 2018, MNRAS, 479, 4017
Inayoshi K., Visbal E., Haiman Z., 2020, ARA&A, 58, 27
Johnson J. L., Dijkstra M., 2017, A&A, 601, A138 (DJ17)
Kreckel H., Bruhns H., Čížek M., Glover S. C. O., Miller K. A., Urbain X., Savin D. W., 2010, Science, 329, 69
Latif M. A., Schleicher D. R. G., Bovino S., Grassi T., Spaans M., 2014, ApJ, 792, 78
Latif M. A., Bovino S., Grassi T., Schleicher D. R. G., Spaans M., 2015, MNRAS, 446, 3163
Martin P. G., Schwarz D. H., Mandy M. E., 1996, ApJ, 461, 265
Neufeld D. A., 1990, ApJ, 350, 216
Oh S. P., Haiman Z., 2002, ApJ, 569, 558
Planck Collaboration VI, 2018, A&A, 641, 67
Regan J. A., Johansson P. H., Haehnelt M. G., 2014, MNRAS, 439, 1160
Regan J. A., Visbal E., Wise J. H., Haiman Z., Johansson P. H., Bryan G. L., 2017, Nat. Astron., 1, 0075
Saslaw W. C., Zipoy D., 1967, Nature, 216, 976
Schleicher D. R. G., Spaans M., Glover S. C. O., 2010, ApJ, 712, L69
Schleicher D. R. G., Palla F., Ferrara A., Galli D., Latif M., 2013, A&A, 558, A59
Shang C., Bryan G. L., Haiman Z., 2010, MNRAS, 402, 1249
Spaans M., Silk J., 2006, ApJ, 652, 902
Stancil P. C., Lepp S., Dalgarno A., 1998, ApJ, 509, 1
Sugimura K., Omukai K., Inoue A. K., 2014, MNRAS, 445, 544
Truelove J. K., Klein R. I., McKee C. F., Holliman J. H. I., Howell L. H., Greenough J. A., 1997, ApJ, 489, L179
Turk M. J., Smith B. D., Oishi J. S., Skory S., Skillman S. W., Abel T., Norman M. L., 2011, ApJS, 192, 9
Visbal E., Haiman Z., Bryan G. L., 2014, MNRAS, 445, 1056
Wise J. H., Regan J. A., O'Shea B. W., Norman M. L., Downes T. P., Xu H., 2019, Nature, 566, 85
Wolcott-Green J., Haiman Z., 2019, MNRAS, 484, 2467
Wolcott-Green J., Haiman Z., Bryan G. L., 2011, MNRAS, 418, 838
Wolcott-Green J., Haiman Z., Bryan G. L., 2017, MNRAS, 469, 3329

APPENDIX A: UPDATED CHEMISTRY RATES

Our chemistry model includes the following updates to the standard ENZO network.

Collisional dissociation of H_2 by H:

We utilize the Martin, Schwarz & Mandy (1996) fit for collisional dissociation of H_2,

$$H_2 + H \rightarrow H + H + H, \tag{A1}$$

including the contribution from dissociative tunneling, which has not previously been used in the ENZO network. Glover (2015a) notes this term becomes larger than direct dissociation at temperatures below 4500 K, and found that neglecting it leads to $J_{\rm crit}$ determinations that are erroneously large by a factor of approximately 2.

Associative detachment of H^- with H:

We use the updated rate coefficient from Kreckel et al. (2010) for the associative detachment reaction:

$$H^- + H \rightarrow H_2 + e^-. \tag{A2}$$

In the sensitivity study by Glover (2015b), this is among the five most important reactions determining $J_{\rm crit}$. The rate from Kreckel et al. (2010) is in good agreement with other recent determinations; however, Glover (2015b) found that the 25 per cent systematic uncertainty results in ~40 per cent uncertainty in $J_{\rm crit}$.

Radiative recombination of H^+:

We use the Case B rate from Hui+Gnedin'97 for the radiative recombination reaction,

$$H^+ + e^- \rightarrow H + \gamma. \tag{A3}$$

This has been previously included as an option in ENZO, but is not always used in primordial chemistry models (e.g. Abel et al. 1997; Shang et al. 2010). In the context of an atomic cooling halo, where the mean-free path for ionizing photons is generally small, using the Case B rate is appropriate. Glover (2015b) notes that the Case A rate is ~60 per cent larger in the relevant temperature range and therefore causes $J_{\rm crit}$ to be ~80–90 per cent smaller in their models.

Radiative association of H and e^-:

We replaced the Hutchins (1976) rate previously used in the ENZO network for the radiative association reaction:

$$H + e^- \rightarrow H^- + \gamma. \tag{A4}$$

We instead use the Abel et al. (1997) rate, whichok agrees well with alternative analytic fits from Stancil, Lepp & Dalgarno (1998) and Galli & Palla (1998) in the range $T = 10^2$–10^4 K, while the Hutchins (1976) rate is significantly larger than the other three at $T \gtrsim 3000$ K. Glover (2015b) finds that $J_{\rm crit}$ results using the Hutchins (1976) rate are nearly a factor of 2 larger than in models using any of the other three rates. Glover (2015b) also notes that the Hutchins (1976) is not valid in the conditions of interest for determining $J_{\rm crit}$ in ACHs, $n \sim 10^3$ cm^{-3}, $T \sim 7500$ K, and therefore recommends against using it in this context.

This paper has been typeset from a TEX/LATEX file prepared by the author.